Nigerian Journal of Applied Physics (NJAP)
ISSN Print: 3115-5871
ISSN Online: 3115-588X
DOI: https://doi.org/10.62292/njap-v2i1-2026-62
Volume 2(1), March 2026

# Construction of Polyvinyl Alcohol (PVAL)-Based Breast Phantoms with Simulated Calcifications and Evaluation of the Effect of Breast Thickness on Radiation Dose in Full Field Digital Mammography

***[1,2]Franca Oyiwoja Okoh, [2]Norlaili Ahmad Kabir, [1]John Actor Ocheje, [1]Moses Ejike Onudibia, [3]Mohd Fahmi Mohd Yusof and [2]Siti Nor Azizah Abdullah**

[1]Department of Pure and Applied Physics, Federal University Wukari, Wukari-Taraba State, Nigeria.
[2]School of Physics, Universiti Sains Malaysia, 11800 Penang, Malaysia.
[3]Faculty of Nursing and Health Sciences, Universiti Islam Melaka, 78200 Malacca, Malaysia.

[*]Corresponding author's email: francaujah2005@fuwukari.edu.ng

**ABSTRACT**
The aim of the present study is to fabricate tissue equivalent breast phantoms with embedded calcification, to investigate their mean glandular dose (MGD) and entrance surface dose (ESD) at various thicknesses using Full Field Digital Mammography (FFDM). Four breast phantoms with embedded calcifications were fabricated using different 10% polyvinyl alcohol (PVAL)-based composites. The first three phantoms were composed of 10% PVAL + ethanol, 10% PVAL, and 10% PVAL + graphite powder, designed to simulate BI-RADS breast density categories 2, 3, and 4, respectively. The fourth phantom was a heterogeneous model constructed by combining the three composite materials in varying proportions. A total of 32 mammographic scans were carried out using AEC (automatic exposure control) mode at different compression force. All exposure parameters were recorded including the applied compression force, MGD and ESD. The study revealed that the compressed phantom thickness (CPT) of all the phantoms investigated ranged from 2.7 to 5.2 cm, MGD ranged from 1.58 – 3.29 mGy (mean = 2.36 ± 0.07) and ESD ranged from 3.7 – 12.33 mGy (mean = 7.10 ± 0.36). The MGD and ESD showed a positive correlation with CPT with r (30) = 0.72, P < 0.0000038 and r (30) = 0.91, P < 0.000001 respectively. The results of the present study are similar to published values, the MGD and ESD are also within the acceptable dose limit recommended by ACR protocol.

**Keywords**:
Breast phantom,
Mammography,
Breast thickness,
Mean glandular dose,
Entrance surface dose.

## INTRODUCTION

Breast phantoms are devices that are used to replace the human breast tissue. Due to the side effects associated with the use of ionizing radiation, phantoms are used to mimic patients in order to carry out dosimetric measurements and quality control / assurance test on medical systems. Commercially available phantoms are often expensive, making them inaccessible to many radiology departments. In addition, most commercially produced phantoms are designed for broad market use and are not customized to meet specific user requirements or applications. Consequently, there is a need to develop low-cost, customized phantoms that can be tailored for particular purposes without compromising their physical and radiological properties within the diagnostic energy range. Such phantoms are important for dosimetric studies and quality control procedures in mammography (Amini, 2018). Microcalcifications are calcium deposits ($< 1\, mm\ in\ diameter$) within the breast tissue which are often an early indicator of breast cancer (Cox & Morgan, 2013). Breast cancer is a worldwide public health problem that accounts for a large percentage of cancer deaths in adult women (Koukou et al., 2015). Early detection through screening with mammography has the tendency to reduce breast cancer mortality (Nakamura et al., 2018). However, since mammography involves the use of x-ray and regular quality control test, the information about the dose received by patients are vital for the optimization of breast imaging procedures. Consequently, the use of breast phantoms with embedded calcification features are recommended for dosimetry and quality control test of mammography equipment.

Dense breast tissues constitute a great challenge to the radiologists as cancers in dense breasts may be mammographically very subtle (Hooley et al., 2012). In view of the importance of breast density in cancer diagnosis and risk assessment, the American College of Radiology (ACR) has established the Breast Imaging Reporting and Data System (BI-RADS). This system classifies breast density on mammography into 4 categories in terms of the amount of fibro glandular and adipose tissue present in the breast. Category 1 breast is almost entirely fat (< 25% fibro glandular tissue), category 2 contain scattered areas of fibro glandular tissue (25 – 50% fibrous tissue), category 3 breast are dense (50 - 75% fibro glandular tissue) and category 4 is extremely dense breast containing more than 75% fibro glandular tissue (D'Orsi, Sickles, & Mendelson, 2013; Gweon, Youk, Kim, & Son, 2013).

In mammography, radiation dose assessment is essential to ensure optimal image quality while minimizing the radiation risk to patients. Two commonly used dosimetric quantities are Mean Glandular Dose (MGD) and Entrance Surface Dose (ESD)**.** MGD represents the radiation dose absorbed by the glandular tissue of the breast, which is considered the most radiosensitive component and therefore the most relevant indicator of radiation risk in mammography. In contrast, ESD refers to the radiation dose delivered to the skin surface of the breast and is often directly measured during dosimetric evaluations. Breast thickness, particularly compressed breast thickness (CBT)**,** is one of the most important factors influencing both MGD and ESD in mammography. During mammographic imaging, the breast is compressed to reduce its thickness, which improves image quality and reduces radiation dose by decreasing tissue attenuation. However, as breast thickness increases, greater X-ray exposure is required to penetrate the tissue and produce diagnostically useful images. Consequently, both MGD and ESD tend to increase with increasing compressed breast thickness.

Recent studies have explored the use of polymer-based materials such as epoxy resin, polyethylene, and polyvinyl alcohol (PVAL) for the development of tissue-equivalent phantoms because of their favorable mechanical properties and radiological similarity to soft tissues (Cournane et al., 2010; Koukou et al., 2015; Ossati, 2015; Prionas et al., 2012). Among these materials, PVAL has demonstrated promising characteristics, including tissue-equivalent attenuation properties, flexibility, and ease of fabrication. However, the use of PVAL in the fabrication of breast phantoms specifically designed to simulate calcifications for mammographic image quality and dose assessment remains limited. This study therefore seeks to fabricate and evaluate PVAL-based calcification breast phantoms of various densities that can simulate breast tissues and calcification structures for the assessment of radiation dose at various breast thicknesses in mammography systems. Such phantoms could provide a cost-effective and reliable alternative for research, dosimetry, and quality control in mammographic imaging.

## MATERIALS AND METHODS

### Fabrication of Calcification from Eggshell

To simulate the round or punctuate type of calcification, chicken eggshells were used. A few cracked eggshells were collected, rinsed thoroughly with water and then soaked in water at room temperature for a period of 2 hours. The inner membranes of the eggshells were gently peeled off and the eggshells were dried in an oven at 100ºC for 1 hour until they become crispy. A blender was used to grind the eggshells and the resulting powder was sieved using a plastic mesh to obtain a fine powder. A few drops of 10% PVAL solution was added to 5 g of the eggshell powder and the mixture was stirred continuously until the powder stick together. The eggshell / PVAL blend was carefully moulded into small balls of approximately 2 - 4 mm diameter using gloved fingers. The prepared calcifications were allowed to dry at room temperature for 48 hours.

### Fabrication of PVAL Calcification Breast Phantoms

The PVAL granules used in this study were obtained from Sigma-Aldrich. The material had an average molecular weight ranging from 85,000 to 124,000 and a degree of hydrolysis greater than 99%. Graphite powder and ethanol solution (99 % with molecular weight of 46.07) were procured from Chemicals and Reagents (C & R) Sdn Bhd. The method of preparation of the PVAL phantoms was in line with previous studies (Okoh et al., 2022; Kabir et al., 2021; Ossati, 2015; Price et al., 2010).

Four different phantoms of thickness 5.5 cm each were fabricated in an attempt to mimic the BIRADS categories of breast tissues. The composition of the phantoms varies, but the process of solidifying the solution to obtain a semi-solid and yet an elastically compressible gel is the same. In each case, the prepared solutions were first cast halfway in the required moulds and refrigerated then the calcifications features were inserted. The balance of the solutions were poured gently into the mould to seal up the calcification and to make up the required thickness. The moulds were covered and frozen again for 12 hours, after which the gels were thawed for another 12 hours. The resulting phantoms were then ready for use and stored in deionised water. Table 1 gives the composition and thickness of all the fabricated phantoms.

**Table 1: Composition and Category of Fabricated Phantoms**

| | Phantom | Composition | Breast type |
|---|---|---|---|
| 1 | PVAL/ethanol calcification phantom (PVAL/E) | 10% wt PVAL/ethanol solution (50g of PVAL granules was dissolved in a 450 ml of solution prepared from equal amount of deionised water and ethanol) | BIRADS 2 |
| 2 | PVAL calcification phantom (PVAL) | 10 wt % PVAL solution (50 g of PVAL granules and 450 ml of de-ionized). | BIRADS 3 |
| 3 | PVAL / graphite calcification phantom (PVAL/G) | 10 wt% PVAL solution and 4% graphite powder (50 g of PVAL, 20 g of graphite powder and 430 ml of deionised water | BIRADS 4 |
| 4 | Heterogenous calcification phantom (PVAL/H) | combination of the 10% PVAl, PVAL/ethanol and PVAL/ graphite in layers | Heterogenous |

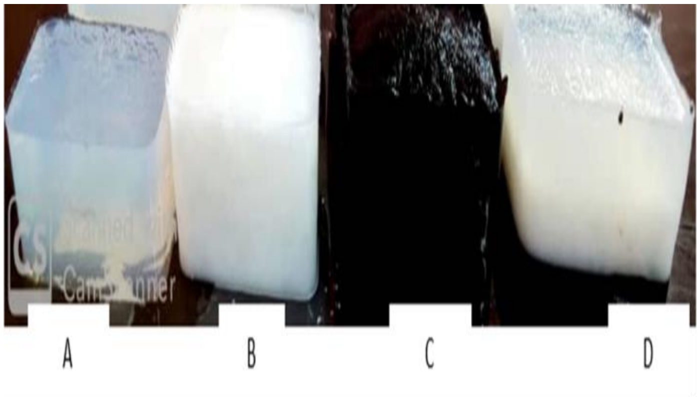


Figure 1: Picture of Fabricated PVAL Composite Phantoms; (a) PVAL/E (b) PVAL (c) PVAL/G and (d) PVAL/H

**Scanning and Dose Assessment**

All phantoms were scanned using the full field digital mammography equipment installed at Hospital Universiti Sains Malaysia (HUSM). The unit was manufactured by hologic selenia dimensions with control panel serial number 81001 143041. The scanning was carried out using the Auto Exposure Control (AEC) mode, which automatically selected the target/filter combinations, tube voltage, current and time for the imaging procedure. A phantom is placed on the breast support platform of the mammography unit and the compression paddle is gently let down until the required amount of force is applied (Figure 2). In this study, we applied compression force in step of 22.7N (5 lbs) resulting in a strain range of 4 -10%, until a force of 181.82 N (40 lbs) was achieved. This is the range of force commonly used in mammography (Price, Gibson, Tan, & Royle, 2010; Waade et al., 2019). The exposure parameters in addition to the compression force, compressed phantom thickness (CPT) mean glandular dose (MGD) and the entrance surface dose (ESD) displayed on the mammography equipment were recorded.

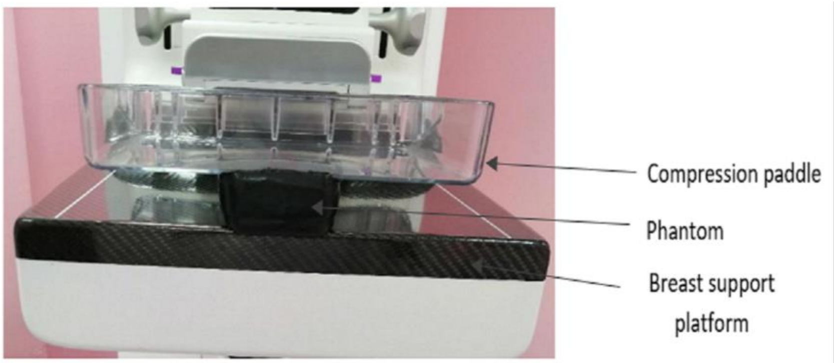


Figure 2: Scanning and Compression Configuration of the PVAL Tissue Equivalent Breast Phantom with the Mammography System

**RESULTS AND DISCUSSION**

Table 2 shows the exposure parameters, CPT, MGD and ESD of 32 mammography scans carried out on the 4 fabricated PVAL phantoms. This data was recorded from the mammography system. The CPT ranged from 2.7 – 5.2 cm (mean = 3.75 ± 0.13), MGD ranged from 1.58 – 3.29 mGy (mean = 2.36 ± 0.07) and ESD ranged from 3.7 – 12.33 mGy (mean = 7.10 ± 0.36). The mean value of the ESD is 3 times higher compared to the mean MGD recorded.

**Table 2: Exposure Parameters, CPT, MGD and ESD for 32 Mammography Scans carried out on the 4 Different Types of Fabricated PVAL phantoms using AEC Mode**

| Phantom | Compression Force (N) | Compressed Phantom thickness (cm) | Tube Voltage (kV) | Tube current-time (mAs) | MGD (mGy) | ESD (mGy) |
|---|---|---|---|---|---|---|
| | 0 | 5.5 | 0 | 0 | 0 | 0 |
| | 22.72 | 4.7 | 28 | 345 | 2.76 | 9.73 |
| | 45.45 | 4.2 | 28 | 300 | 2.61 | 8.32 |
| | 68.18 | 3.8 | 27 | 312 | 2.59 | 7.74 |
| PVAL | 90.91 | 3.6 | 27 | 282 | 2.44 | 6.96 |
| | 113.64 | 3.3 | 26 | 327 | 2.62 | 7.18 |
| | 136.36 | 3.1 | 26 | 305 | 2.54 | 6.66 |
| | 159.1 | 2.9 | 26 | 255 | 2.23 | 5.53 |
| | 181.82 | 2.7 | 26 | 241 | 2.21 | 5.19 |
| | 0 | 5.5 | 0 | 0 | 0 | 0 |
| | 22.72 | 5.1 | 29 | 300 | 2.54 | 9.36 |
| | 45.45 | 4.4 | 28 | 256 | 2.15 | 7.17 |
| | 68.18 | 4 | 28 | 213 | 1.92 | 5.89 |
| PVAL/E | 90.91 | 3.6 | 27 | 214 | 1.85 | 5.28 |
| | 113.64 | 3.3 | 26 | 219 | 1.76 | 4.81 |
| | 136.36 | 3.1 | 26 | 206 | 1.71 | 4.48 |
| | 159.1 | 2.9 | 26 | 188 | 1.64 | 4.07 |
| | 181.82 | 2.7 | 26 | 172 | 1.58 | 3.7 |
| | 0 | 5.5 | 0 | 0 | 0 | 0 |
| | 22.72 | 4.9 | 29 | 371 | 3.22 | 11.5 |
| | 45.45 | 4.4 | 28 | 317 | 2.66 | 8.86 |
| | 68.18 | 4 | 28 | 269 | 2.42 | 7.44 |
| PVAL/G | 90.91 | 3.7 | 27 | 293 | 2.49 | 7.26 |
| | 113.64 | 3.4 | 26 | 312 | 2.45 | 6.87 |
| | 136.36 | 3.3 | 26 | 281 | 2.26 | 6.18 |
| | 159.1 | 3 | 26 | 253 | 2.16 | 5.53 |
| | 181.82 | 2.9 | 26 | 253 | 2.21 | 5.49 |
| | 0 | 5.5 | 0 | 0 | 0 | 0 |
| | 22.72 | 5.2 | 29 | 394 | 3.29 | 12.33 |
| | 45.45 | 4.8 | 28 | 368 | 2.9 | 10.42 |
| | 68.18 | 4.4 | 28 | 324 | 2.72 | 9.06 |
| PVAL/H | 90.91 | 4.1 | 28 | 273 | 2.42 | 7.57 |
| | 113.64 | 3.9 | 27 | 292 | 2.37 | 7.27 |
| | 136.36 | 3.7 | 27 | 282 | 2.39 | 6.98 |
| | 159.1 | 3.5 | 27 | 256 | 2.26 | 6.29 |
| | 181.82 | 3.3 | 26 | 282 | 2.26 | 6.18 |
| Phantom[a] | | 1.0 - 7.0 | 26 - 30 | 16 - 95.3 | 0.48 - 1.73 | - |
| Phantom[b1] | | 4.0 – 6.0 | - | | 1.61 – 3.38 | 6.06 -18.68 |
| Patient[b1] | | 1≤ CBT< 8.0 | | | 1.71 ± 0.45 | 6.60 ± 2.88 |
| Phantom[b2] | | 1.0 -6.0 | 24 - 31 | 17 -259 | 1.61–2.24 | 6.06–9.70 |
| Patient[b2] | | 20 < CBT <80 | | | 1.88 ± 0.33 | 7.94 ± 1.95 |
| PMMA[c] | | 2.0 – 7.0 | | | 0.60 - 3.13 | |

Nakamura et al[a] (2018) Kawaguchi et al[b1] (2012), Kawaguchi et al[b2] (2014) Dance et al[c] (2014)

Figure 3 shows that the distribution of CPT, MGD and ESD fall within the normal distribution with skewness and kurtosis values lying within the acceptable range of -1 to +1 and -2 to +2 respectively for a significance level of <0.05. The data acquired from 32 exposures were analysed in order to observe the relationship between MGD, ESD and the exposure parameters with CPT. The peak of the CPT distribution lies between 3 – 4.9 cm, which is 78.13% of the total sample size, the peak of the MGD distribution lies between 2 – 2.9 mGy, which is also 78.13% of the total sample size and lastly, the peak of the ESD distribution lies between 5 – 8.99 mGy, which forms 68.75% of the entire sample size.

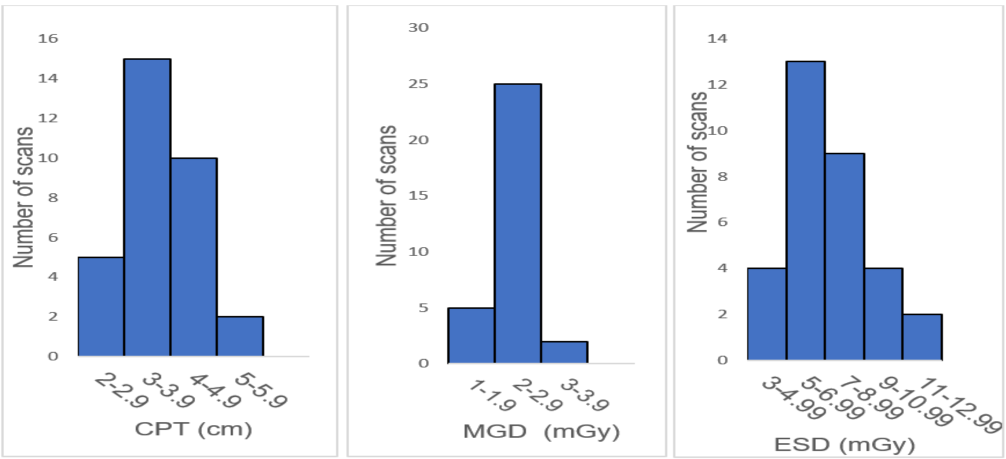


Figure 3: Distribution of the CPT, MGD and ESD for the 32 number of total scans studied

Figure 4 demonstrates that the MGD increases with the CPT. A linear regression test reveals that there is a significant positive relationship between MGD and CPT, r (30) = 0.72, P<0.0000038 and $R^2 = 0.51$. Similarly, the recorded ESDs showed a positive correlation with CPT, r (30) = 0.91, P < 0.000001 and $R^2 = 0.82$. The ESD increases with increase in CPT.

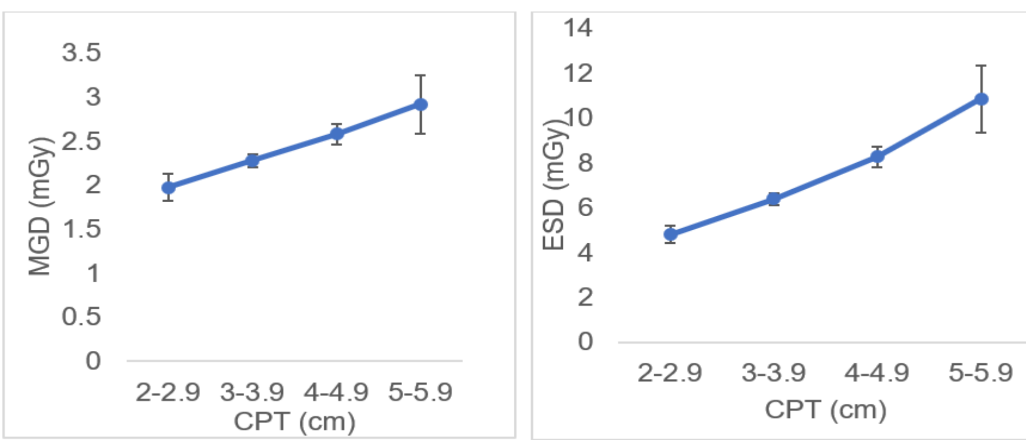


Figure 4: MGD and ESD Values Plotted Against Compressed Phantom Thickness CPT For 32 Mammography Scans. Data Is Presented As Mean ± Standard Error

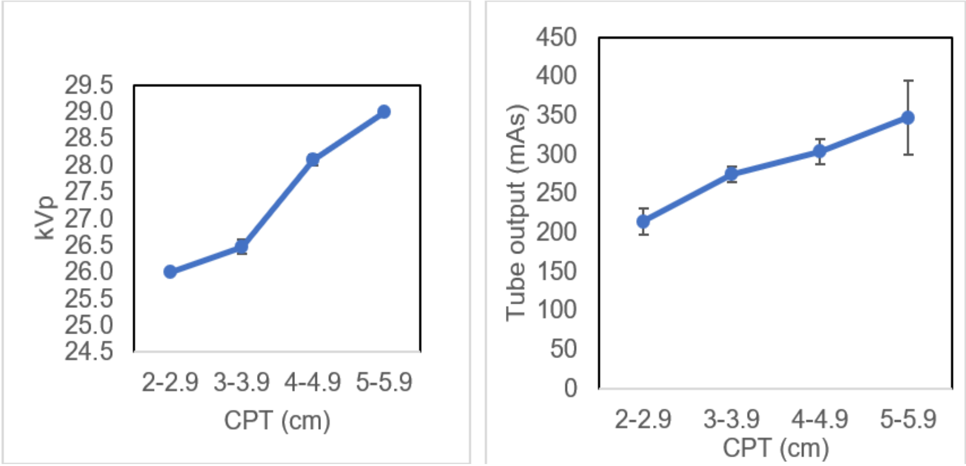


Figure 5: The kVp and mAs Values Plotted against CPT for 32 Mammography Scans. Data is presented as Mean ± Standard Error

**Discussion**

The MGD recorded in this work were found to be in good agreement with published values (Table 2) and also within the acceptable limit of 3.0 mGy consistent with the ACR protocol. Past studies have revealed that the compressed phantom thickness (CPT) could have a significant effect on MGD in mammography (Dance, 1990; Nakamura et al., 2018). This was also reflected in the strong positive correlation of MGD with CPT seen in the present study (Figure 4). Considering the relatively high sensitivity of the glandular tissue in breast to ionizing radiation, many past studies have focused on dose measurement in mammographic procedures. These studies revealed that the MGD could be influenced by many factors (Chevalier et al., 2004; Du, Yu, Zhang, & Wang, 2017; Xiang et al., 2014). Some of the factors are equipment related while others are patient related. The equipment related factors are basically the exposure parameters (kV and mAs) while the patient related factor is the compressed breast thickness.

The observation that PVAL/G and PVAL/H phantoms produced significantly higher mean glandular dose (MGD) and entrance surface dose (ESD) than PVAL/E and pure PVAL phantoms at equivalent compression forces can be attributed primarily to differences in their densities and attenuation properties. In mammography, breast phantoms with higher densities exhibit greater X-ray attenuation, resulting in reduced photon transmission to the detector. To compensate for this increased attenuation and maintain adequate image quality, the automatic exposure control (AEC) system increases the exposure output, typically through higher mAs values. Consequently, both ESD and MGD increase.

As the compressed breast thickness increases, the kVp used during mammographic imaging generally increases. A thicker breast attenuates more X-ray photons due to increased tissue density and path length. Increasing the kVp increases the penetrating power of the X-ray beam, allowing photons to pass through thicker tissue and reach the detector. Mammography typically uses relatively low kVp ranges, usually between 25 and 35 kVp, depending on breast thickness and composition (Bushberg et al., 2012). Modern mammography systems often employ Automatic Exposure Control (AEC) to adjust the kVp appropriately based on compressed breast thickness. As a result, there would be an increase in the ESD of the mammography procedure. Also, as breast thickness increases, more X-ray photons are absorbed or scattered before reaching the detector. Unlike kVp, which affects beam energy and contrast, mAs primarily affects the quantity of radiation and therefore the patient dose. Consequently, increasing mAs for thicker breasts leads to a higher radiation dose. Proper breast compression is therefore essential in mammography because reducing breast thickness decreases the required mAs and helps minimize patient radiation exposure while improving image sharpness. The linear relation of kV/CPT and mAs/CPT displayed in Figure 5 demonstrates that the kV and mAs varied in a similar pattern as CPT increase.

The ESD also showed strong positive correlation with CPT (Figure 4). The reason is that a bigger breast/phantom thickness translates to a higher density perception by the mammography equipment in the AEC mode and would lead to increase in kV and mAs selection. In practice, both kVp and mAs are adjusted together as breast thickness changes.

Breast density plays an important role in mammographic compression because breasts with a higher proportion of fibroglandular tissue are generally less compressible than those with predominantly fatty tissue. Dense breast tissue is structurally firmer and offers greater resistance to compression, which may result in a higher residual compressed breast thickness even when similar compression forces are applied (Bushberg et al., 2012;

Dance et al., 2014). This explains why, despite the application of the same compression force, greater compression was observed in PVAL/E and PVAL, representing BIRADS 2 and BIRADS 3, respectively, compared with PVAL/G and PVAL/H, which represent BIRADS 4 and the heterogeneous breast model, respectively.

## CONCLUSION

This study reports methods to fabricate tissue equivalent breast phantom of various densities with embedded calcifications for mammographic dosimetric assessment using Full Field Digital Mammography (FFDM). The fabricated phantoms exhibited compressed phantom thicknesses ranging from 2.7 to 5.2 cm and were effectively imaged under AEC mode across varying compression forces. A significant positive correlation was observed between compressed phantom thickness and both dose metrics, indicating that increasing phantom thickness leads to a corresponding increase in MGD and ESD during mammographic imaging. This finding is consistent with the known influence of breast thickness on exposure requirements and radiation dose in mammography. Importantly, the dose values obtained in this study were comparable to published data and remained within the acceptable limits recommended by the American College of Radiology (ACR), confirming the dosimetric suitability of the fabricated phantoms.

## REFERENCES

Chevalier, Margarita, Morán, P., Ten, J. I., Fernández Soto, J. M., Cepeda, T., & Vañó, E. (2004). Patient dose in digital mammography. Medical Physics, 161 31(9), 2471–2479.

Cournane, S., Cannon, L., Browne, J. E., & Fagan, A. J. (2010). Assessment of the accuracy of an ultrasound elastography liver scanning system using a PVA-cryogel phantom with optimal acoustic and mechanical properties. Phys Med Biol, 55(19), 5965-5983. https://doi.org/10.1088/0031-9155/55/19/022

Cox, R. F., & Morgan, M. P. (2013). Microcalcifications in breast cancer: Lessons from physiological mineralization. Bone, 53(2), 437-450. https://doi.org/10.1016/j.bone.2013.01.013

D'Orsi, C., Sickles, E., & Mendelson, E. (2013). American College of Radiology (ACR) Breast Imaging Reporting and Data System Atlas (BI-RADS Atlas): American College of Radiology.

Dance, D. R., & Young, K. C. (2014). Estimation of mean glandular dose for contrast enhanced digital mammography: factors for use with the UK, European and IAEA breast dosimetry protocols. Physics in medicine and biology, 59(9), 2127-2137.

Dance, D. R. (1990). Monte Carlo calculation of conversion factors for the estimation of mean glandular breast dose. Phys. Med. Biol., 35(9), 1211-1219.

DeWerd, L. A., & Kissick, M. (2014). The phantoms of medical and health physics: Springer.

Du, X., Yu, N., Zhang, Y., & Wang, J. (2017). The relationship of the mean glandular dose with compressed breast thickness in mammography. Journal of Public Health and Emergency, 1, 32. https://doi.org/10.21037/jphe.2017.03.10

Gweon, H. M., Youk, J. H., Kim, J. A., & Son, E. J. (2013). Radiologist assessment of breast density by BI-RADS categories versus fully automated volumetric assessment. AJR Am J Roentgenol, 201(3), 692-697. https://doi.org/10.2214/AJR.12.10197

Hooley, R. J., Greenberg, K. L., Stackhouse, R. M., Geisel, J. L., Butler, R. S., & Philpotts, L. E. (2012). Screening US in Patients with Mammographically Dense Breasts: Initial Experience with Connecticut Public Act 09-411. Breast Imaging, 265(1), 59-69.

Imam Amini, P. A. a. P. S. (2018). Construction and verification of a physical chest phantom from suitable tissue equivalent materials for computed tomography examination. Radiation Physics and Chemistry.

Kabir, N.A., Okoh, F.O., Mohd Yusof, M.F., 2021. Radiological and physical properties of tissue equivalent mammography phantom: characterization and analysis methods. Radiat. Phys. Chem. 180, 109271 https://doi.org/10.1016/j. radphyschem.2020.109271.

Kawaguchi, A., Kobayashi, M., Otsuka, T., Hattori, S., & Suzuki, S. (2012). Average Glandular Dose and Entrance Surface Dose in Mammography. Radiol Phys Technol, 3(1), 78-85. https://www.irpa.net/members/P07.129fp.pdf

Kawaguchi, A., Matsunaga, Y., Otsuka, T., & Suzuki, S. (2014). Patient investigation of average glandular dose and incident air kerma for digital mammography. Radiol Phys Technol, 7(1), 102–108. https://doi.org/10.1007/s12194-013 0239-9

Koukou, V., Martini, N., Velissarakos, K., Gkremos, D., Fountzoula, C., Bakas, A., Fountos, G. (2015). PVAL breast phantom for dual energy calcification detection. Journal of Physics: Conference Series, 637, 012013. https://doi.org/10.1088/1742-6596/637/1/012013

Nakamura, N., Okafuji, Y., Adachi, S., Takahashi, T., Nakakuma, T., & Ueno, S. (2018). Effect of Different Breast Densities and Average Glandular Dose on Contrast to Noise Ratios in Full-Field Digital Mammography: Simulation and Phantom Study. Radiology Research and Practice, 2018(6192594), 9. https://doi.org/10.1155/2018/6192594.

Okoh F.O., Kabir, N. A., Mohd Yusof, M. F., Mohammed A.S.A, Zainon, R (2022). Investigation of polyvinyl alcohol (PVAL) composite gels and the outcome of variation in breast phantom densities on image quality and dose in full-field digital mammography. Radiation Physics and Chemistry. 200 (110393)

Ossati, M. (2015). Design, development and use of a deformable breast phantom to assess the relationship between thickness and lesion visibility in full field digital mammography. University of Salford Manchester.

Price, B.D., Gibson, A.P., Tan, L.T., Royle, G.J., 2010. An elastically compressible phantom material with mechanical and x-ray attenuation properties equivalent to breast tissue. Phys. Med. Biol. 55 (4), 1177–1188. https://doi.org/10.1088/0031-9155/55/4/018.

Prionas, N. D., Burkett, G. W., McKenney, S. E., Chen, L., Stern, R. L., & Boone, J. M. (2012). Development of a patient-specific two-compartment anthropomorphic breast phantom. Physics in Medicine & Biology, 57(13), 4293.

Surry, K. J. M., Austin, H. J. B., Fenster, A., & Peters, T. M. (2004). Poly(vinyl alcohol) cryogel phantoms for use in ultrasound and MR imaging. Physics in Medicine and Biology, 49(24), 5529-5546. https://doi.org/10.1088/0031-9155/49/24/009

Waade, G. G., Holen, A., Sebuodegard, S., Aase, H., Pedersen, K., Hanestad, B., & Hofvind, S. (2019). Breast compression parameters among women screened with standard digital mammography and digital breast tomosynthesis in a randomized controlled trial. Acta https://doi.org/10.1177/0284185119863989.

Xiang, D. U., Jin, W., Yang, C. Y., Zhou, X. F., Wei, C., Cao, X. J., Zhou, Y. Y., & Le YU, N. (2014). Investigation of mean glandular dose in diagnostic mammography in China. Biomedical and Environmental Sciences, 27(5), 396–399.